European Cells and Materials Vol.54 2025 (pages 65–78) DOI: 10.22203/eCM.v054a05 ISSN 1473-2262

Original Article

THE NEUROVASCULAR AND INFLAMMATORY SIGNATURES OF THE DEGENERATING INTERVERTEBRAL DISC

R.E. Walk[1], K.S. Broz[2], L. Jing[1], R.S. Potter[3], C.E. Gonzalez[1], A.T. Beeve[1,4], E.L. Scheller[1,4], M.C. Gupta[5], L.A. Setton[1,3,5] and S.Y. Tang[1,2,3,5,*]

[1]Department of Biomedical Engineering, Washington University in St. Louis, St. Louis, MO 63130, USA
[2]Institute of Material Science and Engineering, Washington University in St. Louis, St. Louis, MO 63130, USA
[3]Department of Mechanical Engineering and Materials Science, Washington University in St. Louis, St. Louis, MO 63130, USA
[4]Department of Medicine, Washington University School of Medicine, St. Louis, MO 63110, USA
[5]Department of Orthopaedic Surgery, Washington University School of Medicine, St. Louis, MO 63110, USA

Abstract

Objective: Inflammatory cytokine production and de novo neurovascularization have been identified in painful, degenerated intervertebral discs (IVDs). However, the progression of these key pathoanatomical features, including the cascade of inflammatory cytokines and the infiltration of vessels and neurites remain undefined. The objective of this study is to define the progression of cytokine production and neurovascular invasion during the IVD degeneration. **Methods:** A needle-puncture injury model was applied to the caudal IVDs of 3-month-old C57BL6/J female mice. The animals were euthanized after the IVDs were allowed to degenerate *in vivo* for 2-, 4-, and 12-weeks following the injury. A set of IVDs were extracted for immunostaining of infiltrating vessels (endomucin) and nerves (protein-gene-product 9.5). Another set of IVDs were placed in organ culture and forty-nine IVD-secreted cytokines and matrix metalloproteinases (MMPs) were measured from the media. **Results:** IVD injury resulted in severe degeneration by 2-weeks that remained consistent up to 12-weeks post puncture. Injury increased the secretion of interleukin (IL)-6, tumor necrosis factor (TNF)α, C-C motif ligand (CCL)4, CCL12, CCL17, CCL20, CCL21, CCL22, C-X-C motif ligand (CXCL)2 and MMP-2 proteins. Although the control IVDs did not exhibit degeneration, they produced TNFα and CCL22. The centrality and structure of inflammatory networks in IVDs evolves over the 12-week time course following injury, highlighting distinct responses between the acute and chronic phases. Neurites propagates rapidly within 2-weeks post-injury and remains constant until 12-weeks. Vascular length peaks at 4-weeks post-injury and regresses by 12-weeks. These findings identify the temporal flux of inflammatory cytokines and pain-associated pathoanatomy in a model of IVD degeneration of the mouse caudal spine. **Conclusions:** Caudal puncture provides a non-invasive alternative to lumbar puncture allowing for injury to multiple IVDs providing a platform for more extensive studies while minimizing the number of mice needed.

Keywords: Intervertebral disc degeneration, inflammatory cytokines, intradiscal vascularization, innervation, low back pain pathoanatomy.

***Address for correspondence**: S.Y. Tang, Department of Biomedical Engineering, Washington University in St. Louis, St. Louis, MO 63130, USA; Institute of Material Science and Engineering, Washington University in St. Louis, St. Louis, MO 63130, USA; Department of Mechanical Engineering and Materials Science, Washington University in St. Louis, St. Louis, MO 63130, USA; Department of Orthopaedic Surgery, Washington University School of Medicine, St. Louis, MO 63110, USA. Email: simon.tang@wustl.edu.

Introduction

Low back pain affects up to 85 % of the population worldwide [1,2], and intervertebral disc (IVD) degeneration is a significant contributing factor [3,4]. The IVD is a cartilaginous soft tissue and is considered avascular and aneural [5]. Sandwiched between vertebral bodies, the IVD provides resistance against compressive loads and shock absorbance for the axial skeleton. With aging and injury, the IVD degenerates with the compromised ability to perform these essential functions and ultimately leading to low back pain [6]. In addition to the structural collapse and the depletion of proteoglycan-rich matrix, other hallmarks of the degenerating IVD may be culprits to chronic pain, including the production of inflammatory chemokines, expression of catabolic enzymes [7,8], and the invasion of neurites and vessels [9–12]. Chemokines canonically recruit immune cells, which in turn secrete more chemokines that further exacerbate the inflammatory state of the degenerating IVD

[13] and accelerate the breakdown of the extracellular matrix [14,15]. Chemokines produced by the IVD may also contribute to neuron and vessel propagation around and into the annulus fibrosus (AF) which may mediate discogenic low back pain [16]. The chronic presence of these chemokines may sensitize nociceptive neurons to produce more pain signals [17].

Animal models are a common tool for studying IVD degeneration. Injury such as via mechanical overloading [18–21] or needle puncture [22–36] is used to provoke degeneration of the IVD. Though the lumbar spine is more clinically relevant as a site of pain generation, the surgical exposure required to access the lumbar IVD is traumatic, and the surrounding inflammation may confound the IVD-specific responses. In contrast, puncture injury to the caudal IVD can be implemented with relatively simple surgical exposure, with or without radiographic guidance [36]. Furthermore, the murine caudal spine consists of 27 intervertebral discs, compared to just 5 in the lumbar spine [37], and thus a much greater availability of tissues for multiple assays. This also improves experimental robustness through better control of variability by allowing comparisons of IVDs, subjected to different treatment conditions, within the same mouse. Therefore, the caudal spine may be more experimentally efficient for investigating IVD-specific disease mechanisms.

To effectively leverage the advantages of the caudal model, it is crucial to define the progression of the inflammatory cascade and pain-related neurovascular features over time. Both neurites and vessels have been observed in aged mouse lumbar IVDs [38] and in human degenerated IVDs [10], but the time course of how the caudal IVD recapitulates these features is unclear. Therefore, the objective of this study is to define the temporal progression of neurites, vessels, and the local production of chemokines during injury-induced degeneration of the mouse caudal IVD.

Materials and Methods

Animal Model

Three-month-old C57BL6/J female mice (n = 35) were used in this study. They were housed under standard animal husbandry conditions (in a temperature-controlled (21 ± 1 °C) room with normal 12-hour light/dark cycles). Bilateral puncture with 30 G needle of caudal (Coccygeal (Co)) intervertebral discs (IVDs) was performed and adjacent IVDs were used as internal controls (Fig. 1**A**). Pre- and post-procedural X-ray (Faxitron UltraFocus 100, Faxitron Corporation, Tucson, AZ USA) was used to locate the IVDs of interest to confirm puncture. Co4/5 and Co6/7 were injured with Co3/4 and Co7/8 acting as internal controls. A group of animals (n = 5) underwent a sham procedure to create a superficial injury where the only the skin and surrounding soft tissue was punctured without injury to the IVD. Longitudinal assessment of pain behavior and locomotive performance was performed on a subset of animals (**Supplementary Methods**). The mice were euthanized in a CO_2 chamber with 3 % CO_2 for 5 minutes followed by a 2-minute dwell time at 2, 4 and 12 weeks (n = 9–10 per timepoint) after injury; all sham mice were taken out to 12 weeks (Fig. 1**B**). Paired control and injured IVDs from bilateral puncture mice were divided between optimal cutting temperature (OCT) compound embedded histology (Co3/4 and Co4/5; n = 9–10 per timepoint), paraffin embedded histology (Co7/8 and Co6/7; n = 5 per timepoint) and organ culture (Co7/8 and Co6/7; n = 4–5 per timepoint). Sample size was determined from preliminary data of innervation of the IVD following caudal puncture. Sham control and punctured IVDs were divided between immunohistochemistry (Co3/4 and Co4/5) and paraffin embedded histology (Co7/8 and Co6/7). The lumbar dorsal root ganglions (DRGs) were also extracted from a subset of animals and underwent staining for transient receptor potential cation channel subfamily V member 1 (TRPV1) (**Supplementary Methods**). All samples for histology were immediately fixed in 4 % paraformaldehyde (PFA; Fisher Scientific 15710; Saint Louis, MO, USA) in phosphate buffered saline (PBS) at time of sacrifice for 24–48 hours.

Paraffin Embedded Histology

Functional Spine Units (FSUs) containing the Co6/7 and Co7/8 IVDs (n = 5 per timepoint) were used for quantifying the degree of IVD degeneration. Following 24–48 hours in 4 % PFA, spinal segments were demineralized via incubation in 14 % ethylenediaminetetraacetic acid (EDTA) for 10–14 days at room temperature and then dehydrated in increasing concentrations of ethanol. Samples were then embedded in paraffin and 10 μm thick sagittal sections and stained with Safranin-O against FAST Green, applied 4X in 30 second intervals followed by serially graded ethanol (Fig. 1**C**). Stained slides were imaged with NanoZoomer at 20X magnification (Hamamatsu NanoZoomer HT model, Hamamatsu, Japan). IVDs were graded using a standardized 35-point histopathology scale [39]. Briefly, the Melgoza *et al.* [39] system uses a point-based ordinal scale (0–3 for nucleus pulposus (NP) and AF; 0–2 for endplate (EP) and interface) to separately grade NP, annulus fibrosus (AF), EP, and interface regions. Each region is assessed based cellularity, matrix organization, fibrosis, fissures, and boundary integrity between IVD components. The scoring range is based on distinct structural and cellular features, with higher scores reflecting more severe degeneration. Key criteria include changes across different intervertebral disc components. All histological sections were first graded independently by three blinded evaluators, and final scores were determined by consensus.

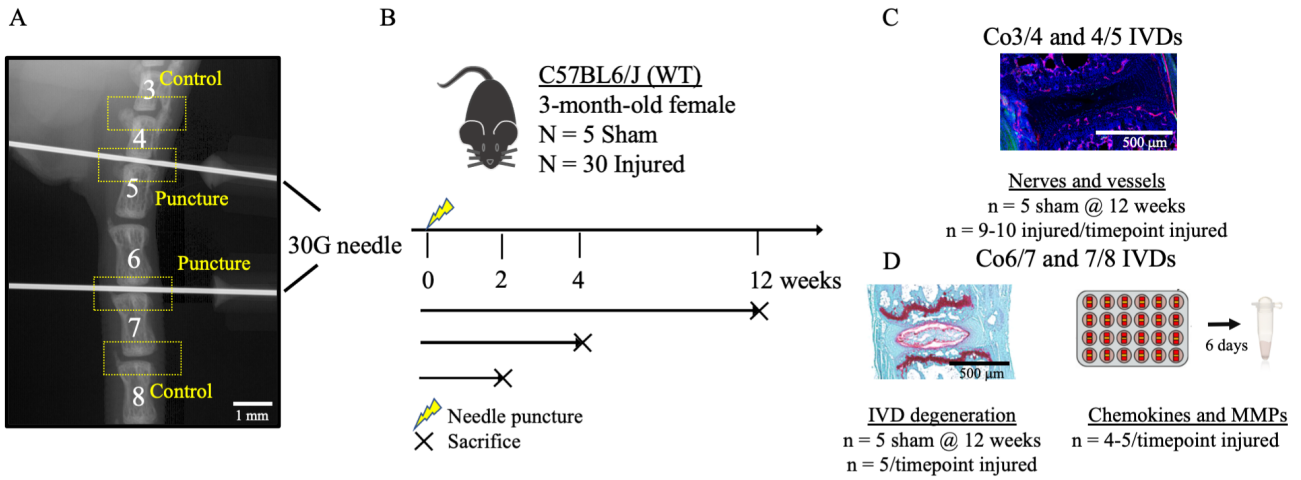

Fig. 1. Bilateral caudal puncture model in female C57BL6/J mice. (**A**) Puncture of Co4/5 and Co6/7 intervertebral discs (IVDs) were confirmed via X-ray, and Co3/4 and Co7/8 IVDs were used as internal controls. The scale bar represents 1 mm. (**B**) Bilateral puncture mice were sacrificed at 2-, 4- and 12-weeks post puncture while all Sham mice were sacrificed at 12 weeks. Sham was a superficial injury limited to the skin and surrounding tissue. (**C**) Immunofluorescence for neurons (green: protein gene product 9.5; PGP9.5) and vessels (red: endomucin (EMCN)) stained against DAPI (blue). The scale bar represents 500 μm. (**D**) Control (Co3/4 and 7/8) and injured (Co4/5 and 6/7) IVDs were divided between Safranin-O against FAST Green staining for IVD degeneration and tissue culture for IVD-specific cytokine and matrix metalloproteases (MMPs) production. Co, Coccygeal; DAPI, 4′,6-diamidino-2-phenylindole. The scale bar represents 500 μm (The illustrations in this figure were created using Microsoft PowerPoint 365).

Quantification of Secreted Factors

FSUs containing the Co6/7 and Co7/8 IVDs (n = 4–5 per timepoint) were cleaned of surrounding soft tissue and immediately placed in tissue culture media at time of sacrifice. Culture media consisted of 1:1 Dulbecco's modified Eagle's medium: Nutrient mixture F-12 (DMEM: F12; Gibco 11320082; Saint Louis, MO, USA) supplemented with 20 % fetal bovine serum (Gibco A5670701) and 1 % penicillin-streptomycin (Gibco 15070063). FSUs were cultured for 6 days at 37 °C and 5 % CO_2 with a complete media change after 3 days. Day 6 media was collected and stored at –80 °C. Aliquots of 200 μL per sample were packaged in dry ice and shipped to Eve Technology for cytokine and matrix metalloproteinase (MMP) analyses (Fig. 1**C**).

The cytokines were measured using the Luminex™ 200 system (Luminex, Austin, TX, USA) using two separate kits, a 32-plex and a Mouse Chemokine Panel 2 assays (MilliporeSigma, Saint Louis, MO, USA) to detect a total of 44 markers. The 32-plex included Eotaxin (C-C motif ligand (CCL)11), granulocyte colony-stimulating factor (GCSF), granulocyte-macrophage colony-stimulating factor (GMCSF), interferon (IFN)-γ, interleukin (IL)-1α, IL-1β, IL-2, IL-3, IL-4, IL-5, IL-6, IL-7, IL-9, IL-10, IL-12 (p40), IL-12 (p70), IL-13, IL-15, IL-17, interferon-γ induced protein (IP)-10 (C-X-C motif ligand (CXCL)10), keratinocyte chemoattractant (KC) (CXCL1), leukemia inhibitory factor (LIF), lipopolysaccharide-induced CXC chemokine (LIX) (CXCL5), macrophage chemoattractant protein (MCP)-1 (CCL2), macrophage colony stimulating factor (MCSF), monokine induced by interferon-γ (MIG) (CXCL9), macrophage inflammatory protein (MIP)-1α (CCL3), MIP-1β (CCL4), MIP-2 (CXCL2), regulated on activation, normal T-cell expressed and secreted (RANTES) (CCL5), tumor necrosis factor (TNF)α, and vascular endothelial growth factor A (VEGFA). Mouse Chemokine Panel 2 assay measured 6Ckine/Exodus2 (CCL21), Erythropoietin (EPO), Fractalkine (C-X3-C motif 1 (CX3CL1)), IFN-β1, IL-11, IL-16, IL-20, MCP-5 (CCL12), macrophage-derived chemokine (MDC) (CCL22), MIP-3α (CCL20), MIP-3β (CCL19), thymus and activation-regulated chemokine (TARC) (CCL17), and tissue inhibitor of metalloproteinases (TIMP)-1. Assay sensitivities of these markers range from 0.3–30.6 pg/mL. Matrix metalloproteases (MMPs) were quantified using a single 5-plex kit (MilliporeSigma). This kit measured MMP-2, MMP-3, MMP-8, proMMP-9 and MMP-12. Assay sensitivities of these markers range from 1.6–8.4 pg/mL. Individual analyte sensitivity values for all kits are available in the MilliporeSigma MILLIPLEX® Multiplex Assay Panel protocol.

Cytokine Network Analysis

To further characterize the temporal variations in inflammatory signaling, networks of cytokine interactions were constructed and visualized using built-in MATLAB functions (Version: 9.13.0.2080170 R2022b, Mathworks, Natick, MA, USA). Networks were generated by calculating a Pearson correlation matrix (corr function) for each timepoint by ratioing each analyte's concentration between injured and uninjured discs for each animal. To focus only

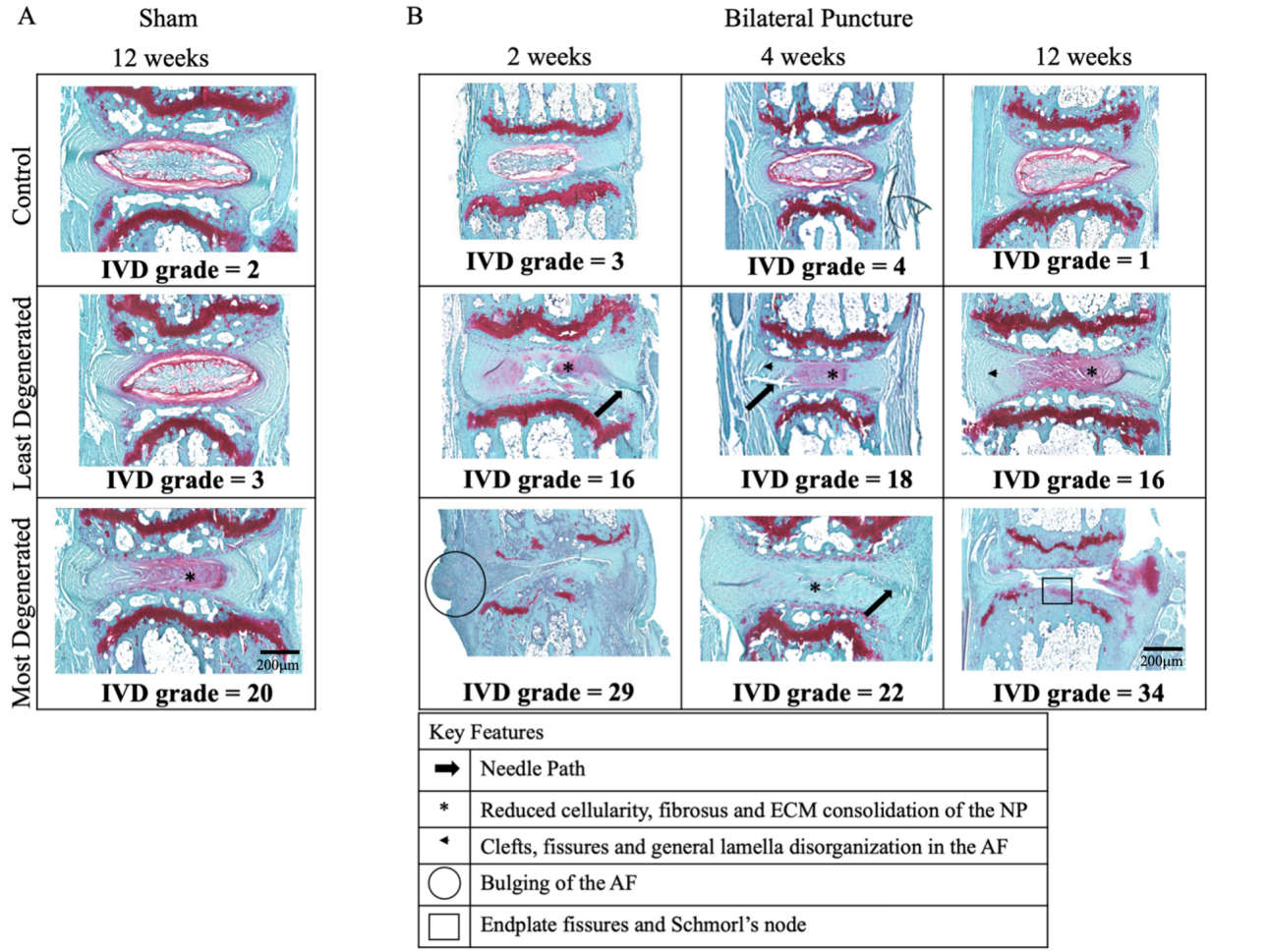

Fig. 2. IVD degeneration is quick and sustained following bilateral puncture of the caudal IVD. Representative Safranin-O-stained sections of a control and the least and most degenerated injured IVD from (**A**) sham and (**B**) bilateral puncture mice at 2, 4 and 12 weeks. Histopathological grading of IVD degeneration ranges from moderate to severe with collapse of the IVD following puncture. The scale bar represents 200 μm. (**C**) Total degenerative grade was significantly increased at 2, 4 and 12 weeks after injury compared to internal control which was not seen in sham. (**D**) Compartmentalized differences in degeneration between control and injured IVDs was seen in the nucleus pulposus (NP), annulus fibrosus (AF) and at the interfaces while the cartilagenous endplates (CEPs) were only significantly different between injury and control at 12 weeks (a indicates $p < 0.05$ compared to internal controls). No degeneration was observed to the IVDs adjacent to the injury. Data (**A,B**) were statistically analyzed via paired two-way ANOVA with the post-hoc Turkey's honest significance test (HSD) for control vs. injured. ANOVA, analysis of variance; ECM, extracellular matrix. ***$p < 0.001$ and ****$p < 0.0001$. This figure was partially created using GraphPad Prism and assembled using Microsoft PowerPoint 365.

on strong protein correlations, a threshold (|r| >0.7) was applied to the correlation matrices and self-directed edges were removed. The filtered matrices were used to create undirected graphs, with nodes representing cytokines and edges representing correlations superseding our aforementioned threshold. Eigenvector centrality and between-

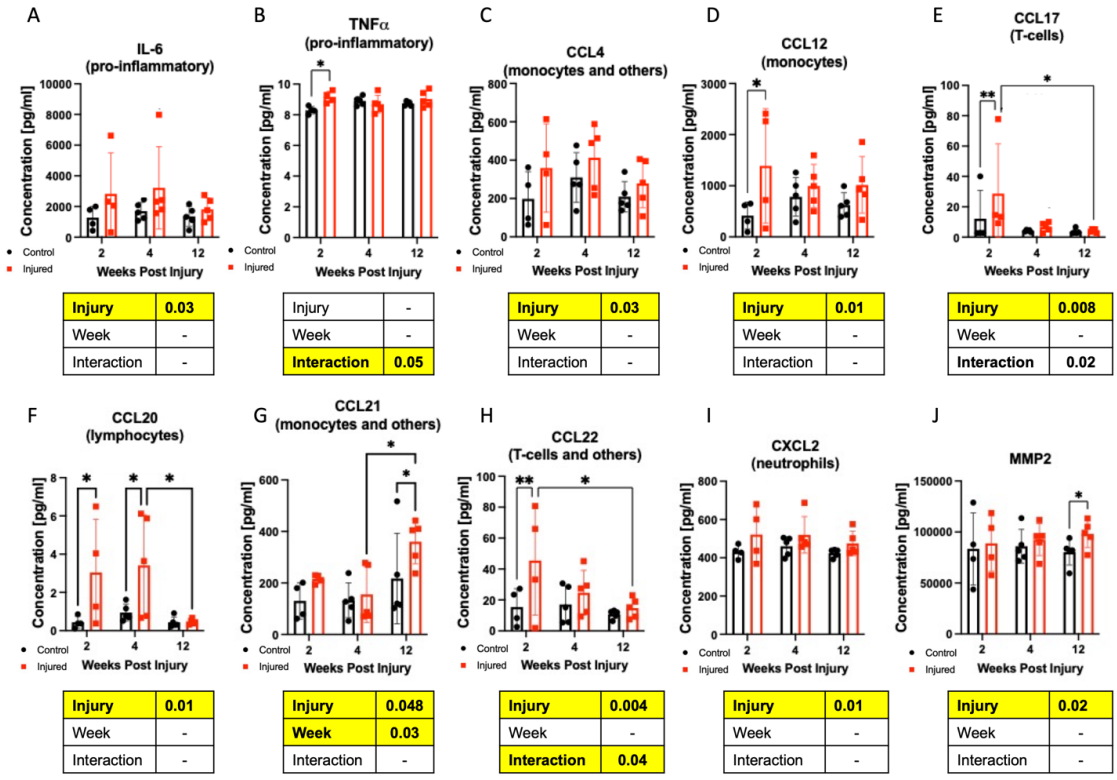

Fig. 3. The injured IVD increased cytokine and MMP production. The measured chemokines can be broadly characterized into 2 categories: pro-inflammatory and immune cell recruitment. Immune cell recruitment chemokines are further labeled by their canonical functions. Pro-inflammatory cytokines (**A**) IL-6 is increased with injury while (**B**) TNFα peaks at 2 weeks following injury. There were also increases in chemokines associated with monocytes, (**C**) CCL4 and (**D**) CCL12. (**E**) CCL17 is associated with lymphocytes. (**F**) CCL20 is and associated with neutrophils. (**G**) CCL21 is associated with T-cells. (**H**) CCL22 is associated with lymphocytes. (**I**) CXCL2 is associated with neutrophils. (**J**) MMP-2 was the only of the five MMPs measured that was elevated with injury. Although the control IVDs did not exhibit degeneration, they produced TNFα and CCL22. Post-hoc comparisons (Tukey's HSD) where the *p*-value is less than 0.05 and less than 0.01 are denoted by * and **, respectively. The *p*-values of the main effects and their interactions are listed in tables below the corresponding graph when they are equal to or less than 0.05. IL, interleukin; TNF, tumor necrosis factor; CCL, C-C motif ligand; CXCL, C-X-C motif ligand. This figure was partially created using GraphPad Prism and assembled using Microsoft PowerPoint 365.

ness centrality were computed using the built-in centrality function to determine important cytokines for each network. High-ranking cytokines shared between timepoints and unique to each timepoint were identified through set operations (intersect and setdiff functions). Additionally, key network characteristics were extracted to understand the structure and function of the cytokine networks. The path length was computed as an average of the shortest finite paths between all pairs of nodes; modularity was computed using the Louvain community algorithm [40]. The Jaccard index calculated for all pairs of networks with 2-hop reachability matrices to allow for quantifying similarity between networks with a slight tolerance for indirect edge comparisons, all of which was done through matrix arithmetic and set operations as previously mentioned. Finally, networks were visualized using force-directed layouts (graph function) with nodes colored by eigenvector centrality and sized by betweenness centrality.

Evaluation of Intradiscal Vascularization and Innervation

The FSUs including Co3/4 and Co4/5 IVDs (n = 9–10 per timepoint) were used for neurovascular staining. These spinal segments following 24–48 hours incubation in 4 % PFA at 4 °C were demineralized for 3 days in 14 % EDTA, embedded in O.C.T. Tissue-Plus Compound (Fisher Scientific 23-730-571; Saint Louis, MO, USA) and placed into a –80 °C. Embedded samples were sectioned on a cryostat at 50 μm thickness. Frozen sections were stained with anti-protein gene product 9.5 (PGP9.5; abcam AB1761-I; Waltham, MA, USA; 1:1000) and anti-endomucin (EMCN; eBio 14-5841-85; San Diego, CA, USA; 1:500) against 4′,6-diamidino-2-phenylindole (DAPI) (Invitrogen D1306; Waltham, MA, USA; 1:1000). Hydrophobic pens were used create boundaries for the antibodies. Primary antibodies were left on for 4 hours in room temperature, while secondary antibodies were applied over night at 4 °C. PGP9.5 is a neuronal marker for sensory and autonomic nerve fibers

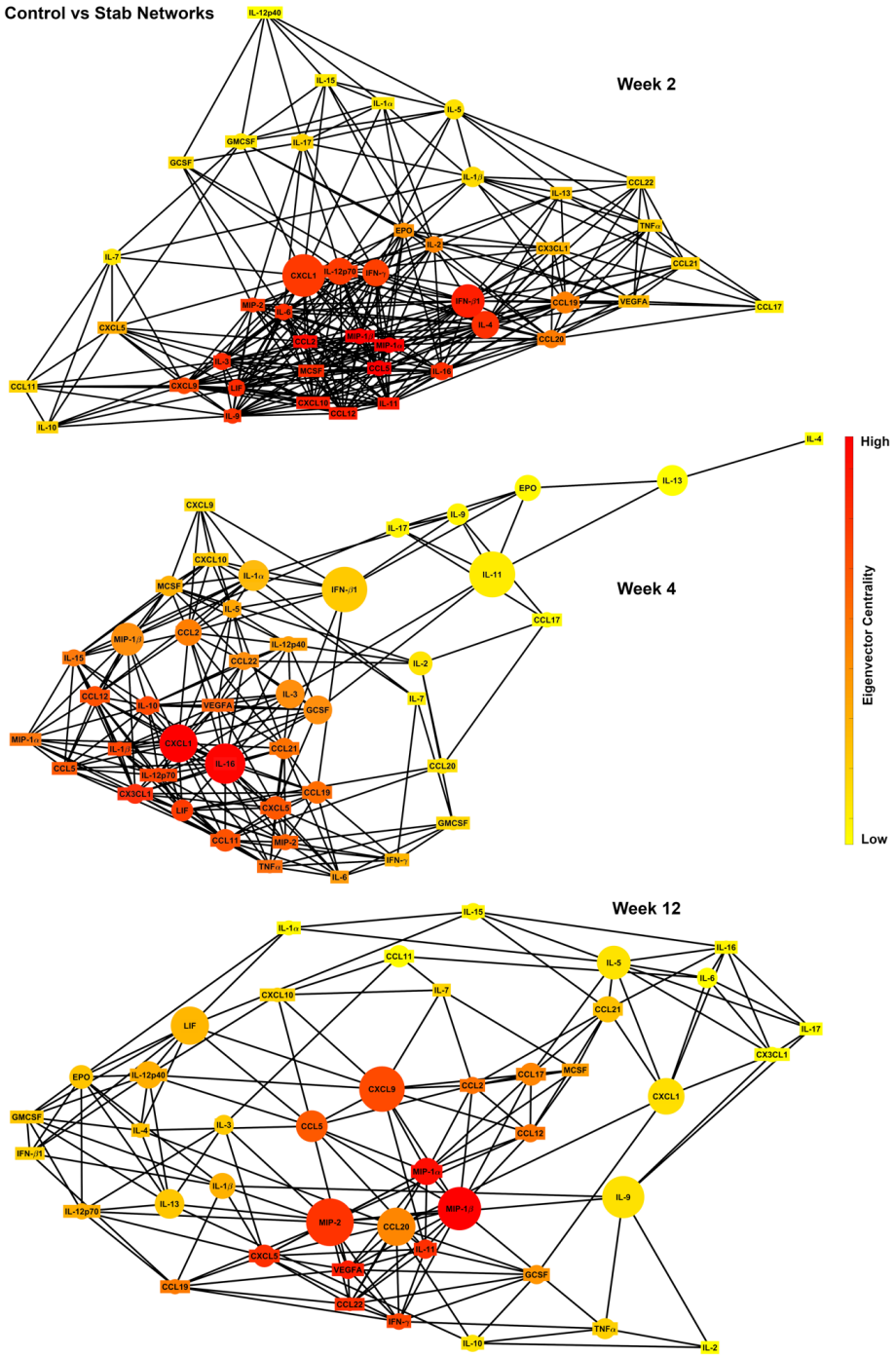

Fig. 4. Evolution of cytokine network structure over time following injury highlights distinct acute and chronic inflammatory phases. At 2 weeks post-injury, a diverse range of pro-inflammatory and immune-recruiting cytokines (IL-4, IFN-γ, CCL2, CCL5) showed high centrality, reflecting the peak up-regulation of cytokines during the acute inflammatory phase. By 4 weeks, while some immune-recruiting cytokines (IFN-β1, IL12p70, CXCL1) maintained central roles, additional chemotactic and immune-regulating factors (CX3CL1, IL-16, LIF) emerged, indicating a transition in the network toward chronic inflammatory processes. At 12 weeks, cytokines involved in angiogenesis and late-stage inflammation (CXCL2, CCL17, CCL20) became highly central, suggesting a latent transition toward a chronic inflammatory microenvironment. Throughout all time points, CCL4 remained highly central, indicating its potential role in both early and chronic inflammation, while IL-11 also consistently ranked highly. Increasing network modularity and path length over time reflected a shift from parallel acute inflammatory pathways to more distinct and linear chronic regulatory relationships, with week 12 being markedly different from earlier timepoints. EPO, Erythropoietin; IFN, interferon; LIF, leukemia inhibitory factor; GCSF, granulocyte colony-stimulating factor; GMCSF, granulocyte-macrophage colony-stimulating factor; MIP, macrophage inflammatory protein; MCSF, macrophage colony stimulating factor; CX3CL1, C-X3-C motif 1; VEGFA, vascular endothelial growth factor A. This figure was created using MathWorks Matlab R2022b.

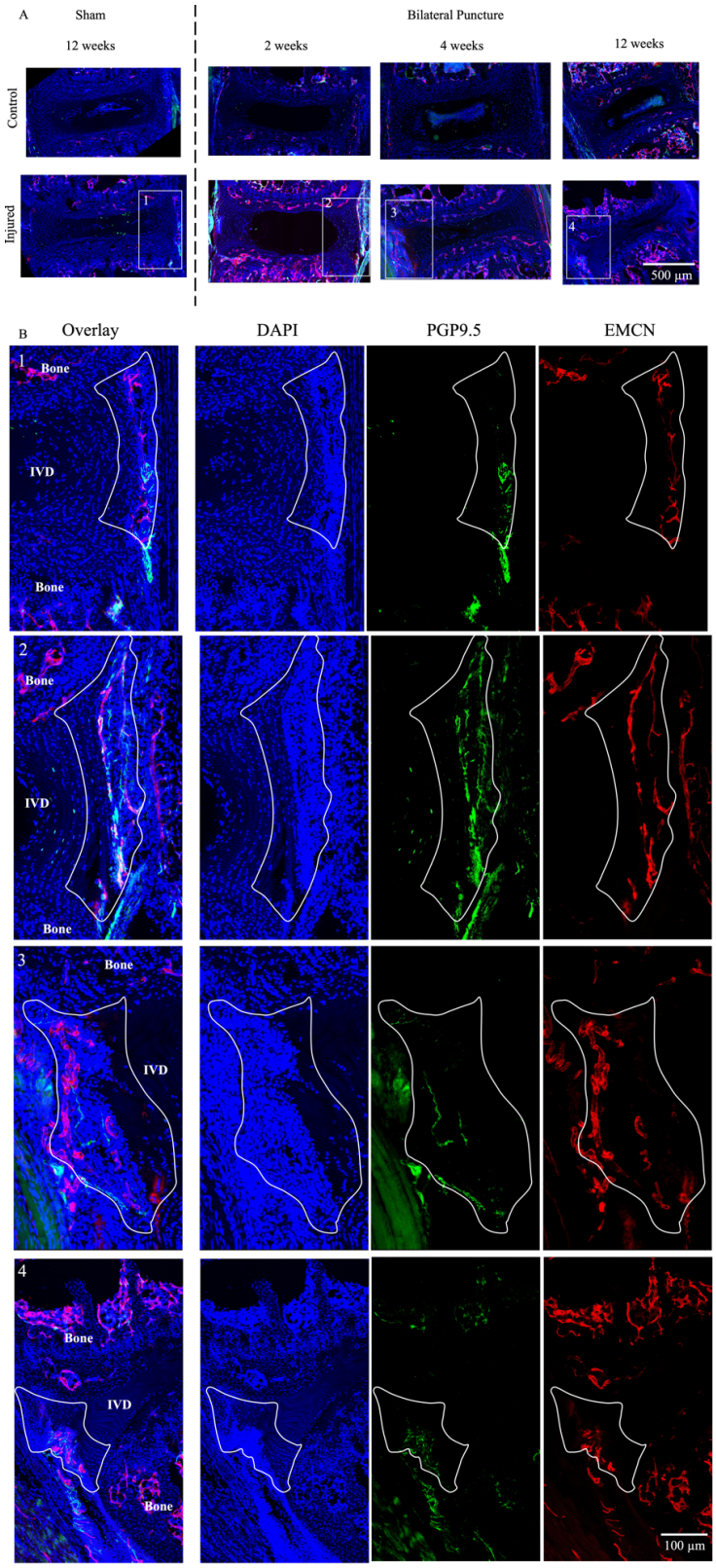

Fig. 5. Representative images showing infiltration of neurites and vessels. (**A**) Maximum projection immunofluorescence images stained with PGP9.5 (green) and EMCN (red) against DAPI (blue) from sham and bilateral puncture mice. Control and injured are paired samples. Both the medial and lateral sides of the IVD are semi-automatically traced in ImageJ and used for further analysis. The scale bar represents 500 μm. (**B**) Zoomed in regions from injured IVDs (sham and bilateral puncture). ROI, circled in white, includes the outer annulus fibrous and surrounding disorganized tissue. The scale bar represents 100 μm. PGP9.5, protein gene product 9.5; ROI, region of interest. This figure was assembled using Microsoft PowerPoint 365.

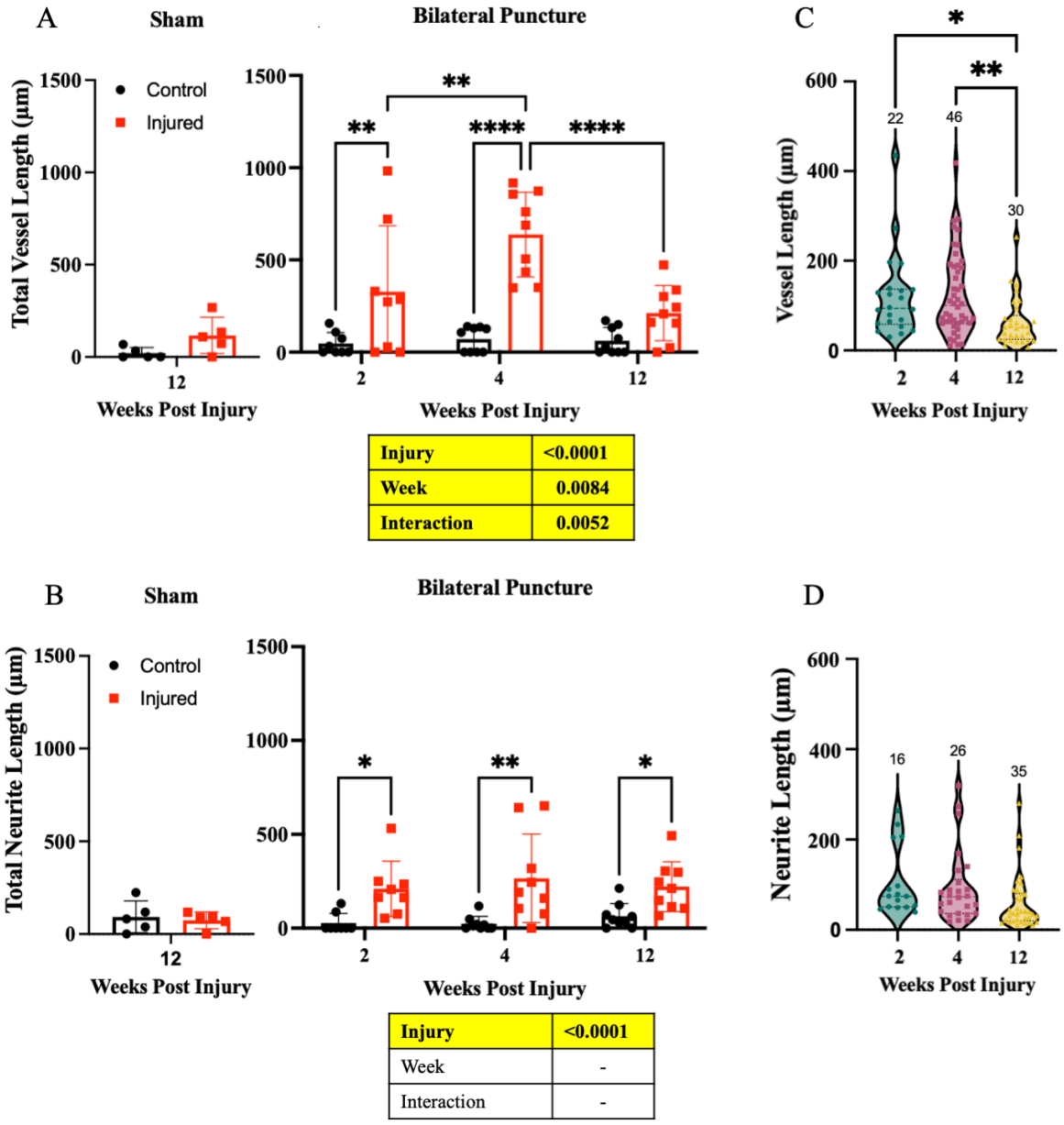

Fig. 6. Quantification of vessel and neurite lengths reveal divergent temporal progression of these features. All individual vessels and neurites were semi-automatically traced and their lengths tabulated. The total length (sum of all individual lengths) of (**A**) vessels and (**B**) nerves demonstrated the presence of both structures in the IVD as early as 2 weeks after injury. Infiltrating vessels peaked at 4 weeks and appeared to recede by 12 weeks after injury, compared to nerves which remain consistently present through all 12 weeks. The violin plots of the bilateral punctured IVDs of (**C**) vessel and (**D**) nerve length demonstrated that the decreased total vessel length was mainly due to a reduced number of longer vessels compared to both 2 and 4 weeks after injury. Number of vessels/nerves traced written above violin plots. *$p < 0.05$, **$p < 0.01$ and ****$p < 0.0001$. p-values of main effects and interaction ($^{-}p > 0.05$) listed in tables below corresponding graph. This figure was partially created using GraphPad Prism and assembled using Microsoft PowerPoint 365.

and EMCN is an endothelial cell marker (Fig. 1**D**). Visualization of PGP9.5 and EMCN was achieved with Alexa Fluor 488 (green; Jackson Immuno Research 711-545-152; West Grove, PA, USA; 1:500) and Alexa Fluor 647 (red; Jackson Immuno Research 712-605-153; West Grove, PA, USA; 1:500) antibodies, respectively.

Three-dimensional image stacks were obtained via confocal fluorescence microscopy (DMi8, Leica Microsystems, Wetzlar, Germany) and a maximum intensity image of each 50 μm section was generated for analysis. Nerves and vessels were semi-automatically traced using ImageJ 2.3.0 (National Institutes of Health, Bethesda, MD, USA) simple neurite tracer (SNT) plugin [41]. Individual struc-

ture lengths were tabulated and then total neurite and vessel length was calculated from the posterior and anterior sides of the IVD. The outer annulus fibrosus and immediately adjacent tissues were included as the region of interest (ROI) for quantification.

Statistics

Because there is a control (uninjured) and an injured spine segment within each animal, we utilized the paired two-way analysis of variance (ANOVA) to test for an effect of IVD injury and duration of the injury on the outcome measures. A paired two-way ANOVA was used to test for an effect of injury and week post-injury between the experimental and control segments, at a significance level of 0.05 with a post hoc Tukey honest significance test (HSD) (Prism 10.2.2, GraphPad, San Diego, CA, USA). A paired *t*-test was used to test for an effect of the superficial injury on experimental levels vs. control segments in the sham-injured group only (12 weeks).

Results

Direct Injury to the Intervertebral Disc Causes Rapid and Sustained Degeneration

Bilateral puncture of the caudal intervertebral disc (IVD) resulted in mild to severe histopathologic degeneration (Fig. 2**A**). Complete collapse of the IVD was observed in the most severe cases. Co6/7 and Co7/8 IVDs from sham and bilateral puncture mice were graded on a histopathologic scale for IVD degeneration and total IVD grade was significantly increased in punctured IVDs compared to internal controls of injured ($p < 0.05$, ANOVA) but no differences were detected in these levels in the sham mice ($p = 0.1$, *t*-test; Fig. 2**B**). Multiple compartments of the IVD showed degenerative changes, including the nucleus pulposus, annulus fibrosus and the interfaces at all timepoints after injury while cartilaginous endplates (CEPs) were only significantly degenerated at 12 weeks following injury (Fig. 2**C,D**). No degeneration appears to have occurred in the adjacent control IVDs. No effect of injury was observed in any pain behavior or locomotive assessments (**Supplementary Fig. 1**).

Cytokine Production Peaked at 2 Weeks after Injury

Forty-four distinct cytokines and five MMPs were measured from the culture media of control and punctured functional spinal units from injured mice. An effect of injury was seen in both pro-inflammatory cytokines (IL-6 and TNFα) and immune cell recruitment chemokines (CCL4, CCL12, CCL17, CCL20, CCL21, CCL22 and CXCL2) (Fig. 3). The greatest difference between injured and control IVDs in chemokine production occurred 2 weeks after injury where significantly higher expression of CCL12, CCL17, CCL20, CCL22 and TNFα with all but CCL20 returning to control levels by 4 weeks post injury and CCL20 by 12 weeks post injury (Fig. 3**A–E**). CCL21 was elevated at 12 weeks after injury (Fig. 3**G**). MMP-2 was detected as being affected by injury with the peak at 12 weeks post injury (Fig. 3**J**). Two cytokines were not detectable in most samples, while 32 cytokines were not different with injury (**Supplementary Table 1**).

Correlative Network Analysis Reveals Key Molecular Hubs Central to the Chemokine Flux

There were several novel findings in identifying influential cytokines in the networks across the 3 timepoints in this study (Fig. 4). At 2 weeks post injury, pro-inflammatory (IL-4) and immune-cell recruiting (IFN-γ, CCL2, CCL5) cytokines high ranked in centrality. By week 4, these were no longer highly central, but IFN-β1, IL12p70, and CXCL1 (which are immune-cell recruiting cytokines also highly central in the week-2 network) were still high-ranking nodes in centrality measures. Additional chemotactic and immune-cell regulating cytokines (CX3CL1, IL-16, and LIF) were highly influential in the network at week 4. In moving to week 12, a unique set of cytokines and pleiotropic factors (IL9, CXCL2, CXCL9, CCL17, CCL20, and vascular endothelial growth factor A (VEGFA)) were central to network activity. Throughout all time points, IL-11 and CCL4 were consistently highly ranked in both centrality measures. In analyzing the network characteristics, modularity greatly increases as time progresses after injury (0.269, 0.368, 0.466 for week 2, 4, 12 respectively). These findings were corroborated by the increase in path length as time progresses (1.41, 1.69, and 1.80), wherein regulatory relationships became more distinct and linear while being less interactive and autoregulatory at later timepoints. In comparing network intersections, week 2 and week 4 are the most similar (0.327 Jaccard Index) while week 2 vs. week 12 and week 4 vs. week 12 are equally dissimilar (0.238 and 0.237 Jaccard Index respectively).

Innervation and Vascularization Propagate at Different Temporal Trajectories

PGP9.5+ neurite and EMCN+ vasculature structures were manually segmented on a maximum projection image (Fig. 5**A**). The region of interest (ROI) contained the anterior and posterior outer annulus fibrosus and surrounding tissue. High magnification ROIs showed innervation and vascularization that colocalized in these areas (Fig. 5**B**). Nerve and vessel structures were semi-automatically traced and lengths were tabulated in each IVD.

Sham mice showed negligible amounts of innervation and vascularization within their IVDs. Total length of each feature in each IVD was measured and an increased presence of both structures was observed as early as 2 weeks after injury (Fig. 6**A,B**). PGP9.5+ neurite structures were observed 2 weeks following injury and remain consistently increased through the 12 week period; in comparison, EMCN+ vessels peaked at 4 weeks and appeared to recede

by 12 weeks after injury. The violin plots showed the tabulation of individual nerve and vessel lengths and the total above each group (Fig. 6**C,D**). The distribution of nerves remained consistent through all 12 weeks while the number of vessels in the 150–300 μm range was dramatically reduced at 12 weeks compared to 4 weeks post injury.

Discussion

IVD injury models are a commonly utilized tool for studying the progression of IVD degeneration, and in the model here we observed the increased expression of TNFα consistent with prior reports [42,43]. Injury to the lumbar IVD also evokes changes in pain behavior [35,44–46]. However, we did not observe notable behavioral changes following injury in the caudal spine (**Supplementary Fig. 1**). Yet, the accessibility caudal IVDs means that multiple levels can easily be injured in a single mouse, allowing for more extensive studies on IVD injury response, while promoting the reduction in the number of research animals used in accordance to the 3R principle [47]. The use of the caudal spine also minimizes the interference due to the disruption and inflammation of surrounding tissues compared to the complex surgical access to the lumbar spine. While there have been extensive studies showing the structural and compositional degenerative changes following caudal puncture [27,28,36,48,49], limited data exists on these additional aspects of IVD degeneration including innervation [25,26] and vascularization and IVD-specific cytokine secretion [50,51]. Our results here show that the caudal IVD produces diverse cytokines, and it is susceptible to developing pain-associated features after injury.

Bilateral puncture of the caudal IVD resulted in quick and sustained IVD degeneration. Both pro-inflammatory cytokines (IL-6 and TNFα and chemokines (CCL4, CCL12, CCL17, CCL20, CCL21, CCL22 and CXCL2) were elevated with injury, with the highest number of produced chemokines at 2 weeks following injury compared to controls. Of note, these cytokines are specifically produced by the IVD during organ culture, and there may have been other systemically elevated cytokines evoked by the injury not expressed by the IVD. The chemokines detected here are canonically known to recruit monocytes, T-cells, and lymphocytes [52]. Yet many chemokines are also known to be pleiotropic and can further instigate IVD degeneration, pain, neurite growth and angiogenesis, either directly within the IVD cells, or indirectly by exerting actions on neurons, endothelial cells, and immune cells [8,17,53]. For example, CCL4 has been shown to be elevated in degenerated human IVDs and associated with pain behavioral changes in a rat model of IVD degeneration [8,54,55]. TNFα injected into rat lumbar IVDs has been shown to enhance pain behavior changes, possibly through irritation of nerve endings [31]. CCL21 induced dorsal root ganglion (DRG) axonal growth [56,57] and CXCL2 is a known mediator of angiogenesis [57,58]. CCL17 and CCL22, acting through the receptor CCR4, play a role in pain development, while CCL22 can activate neurons through increasing excitability [59]. Chemokines production of the IVD following injury may help provide further insights into the pathoanatomy of innervation and vascularization as well as provide possible pathways for IVD degeneration associated low back pain. More work is required to define the cell-specific actions as well as to disentangle the crosstalk between disparate cell types.

Correlative network analysis of the cytokine production revealed several central factors in both the acute and chronic phases of injury. CCL4, a factor significantly upregulated in the IVD within this injury model, is highly central in the cytokine network at all time points. Thus the CCLs may be a crucial hub protein that plays a critical role the progressive inflammation. This highlights two distinct regimes of chronic inflammatory degeneration within the IVD. The correlative network analysis also reveals that CCL4 may be a target for early intervention given its consistent influence on the expression of other cytokines, elevated expression during injury, and its suggested role in IVD degeneration and pain development previously mentioned. On the other hand, CXCL2, CCL17, and CCL20 may be more appropriate as targets of late-stage intervention in chronic painful degeneration of the disc, given their aforementioned roles in angiogenesis, pain development, immune cell recruitment. Network comparison revealed that both modularity and path length increase greatly with time after injury. This suggests that earlier timepoints are characterized by a broad variety of inflammatory pathways functioning in parallel (a notion supported by the peak upregulation of cytokines at 2 weeks post injury). In contrast, later timepoints are characterized by a more specific and linear set of chronic cytokine relationships. This is further supported by the network similarity scores, with week 12 being highly dissimilar from week 2 and week 4. This ultimately suggests that the microenvironment of the injured IVD switches from promoting acute inflammation to promoting chronic inflammation between week 4 and week 12, which could serve as the critical window for the mechanistic underpinnings of chronic inflammatory signaling to develop.

Innervation of the IVD may be the potentiator of low back pain observed with lumbar puncture models and this feature is recapitulated here in the caudal spine. Studies have previously illustrated innervation of the IVD following injury with detection of PGP9.5+ or CGRP+ staining injured IVDs, but without any quantification of the structures [22,24,26]. Further, the coincidence of vascularization with neo-innervation has been previously observed [38], but the time course of vessel propagation into the IVD following injury has not been documented. To overcome these limitations, we semi-automatically traced neurite and vascular structures on maximum projection images of PGP9.5 and EMCN stained thick sections using a software toolbox

for quantifying neuroanatomy [41]. While this analysis expands on previous studies mentioned above, future work can further assess the three-dimensional (3D) morphology and the spatial orientation of these structures. This allowed for the tabulation of neurites and vessels present in the region of interest and their lengths for comparison. We observed a time-dependent vessel infiltration of the outer annulus fibrosus and surrounding tissue. In contrast, neurites quickly infiltrated within two weeks of injury and remained at similar levels in the subsequent weeks. It is likely that the penetration of the IVD by vessels would be considered prerequisite to infiltration by circulating cells, including monocytes and other immune cells that might be responsible for secretion of the cytokines.

Behavioral assays can be used following lumbar puncture to quantify pain [23,24,34,35]. A caveat of the caudal puncture model is that it does not produce axial low back pain. Correspondingly, we observed no differences in behavioral measures between sham and bilateral puncture mice. Although not measured here, there may have been localized measures of pain including sensitization of the tail to mechanical and thermal stimuli (e.g., the Hargreaves test or the tail-flick test) [26,60]. Another surrogate of pain-related change is to quantify molecular expression of neurotrophic factors in the innervating lumbar dorsal root ganglion (DRG). The DRG has been linked to chronic pain, and the increase in the expression of pain-related neuropeptides as well as neuronal excitability may be the mediators of discogenic pain [61]. Transient receptor potential cation channel subfamily V member 1 (TRPV1) is elevated in the DRGs taken from mice with caudal IVD injuries, confirming that there may be a chronically pain-inducing stimuli in the upstream DRGs (**Supplementary Fig. 2**).

The method for quantifying innervation and vascularization of the IVD enabled measuring these features with enhanced fidelity. Protein analysis of the IVD secreted chemokines revealed potential molecular mediators of IVD degeneration, innervation and vascularization relevant to inflammation and pain. Many of the secreted chemokines are associated with increased presence of infiltrating monocytes that may include macrophages, B-cells or T-cells [62,63]. In this study, we intentionally measured locally produced cytokines which will remove the effects of systemic changes in the animal. Recent work shows that the chronic nuclear factor kappa B (NFκB) activation in the caudal IVD produces a secretome that promote macrophage migration [64]. The IVD injury also recruits multiple immune cell types in this model [62], consistent with concomitant increased chemokine production and neurovascular features of the IVD observed in this study. Future studies quantifying the presence of these immune cells would advance our understanding of a role for local vs. systemic changes in modulating chemokine secretion, as well as key factors that govern the infiltration of these pain-associated features.

Conclusions

Caudal puncture provides a non-invasive alternative to lumbar puncture to study the injury response of the IVD. Here, we quantified the neurovascular response and evaluated a cytokine signature of the injured IVD. Our results demonstrated time dependent infiltration of neurovascular structures and excreted cytokines. While standard measures to quantify pain are not useful in this model, alternative techniques can be utilized in future studies. In addition, future work investigated the function of the excreted chemokines and immune response may provide insight into potential mechanisms of discogenic low back.

List of Abbreviations

AF, annulus fibrosus; CEPs, cartilaginous endplates; CCL, C-C motif ligand; CXCL, C-X-C motif ligand; Co, Coccygeal; EMCN, endomucin; GCSF, granulocyte colony-stimulating factor; GMCSF, granulocyte-macrophage colony-stimulating factor; IFN, interferon; IL, interleukin; IP, interferon-γ induced protein; IVD, intervertebral disc; KC, keratinocyte chemoattractant; LIF, leukemia inhibitory factor; LIX, lipopolysaccharide-induced CXC chemokine; MCP, macrophage chemoattractant protein; MCSF, macrophage colony stimulating factor; MDC, macrophage-derived chemokine; MIG, monokine induced by interferon-γ; MIP, macrophage inflammatory protein; MMP, matrix metalloproteinase; NFκB, nuclear factor kappa B; NP, nucleus pulposus; PGP9.5, protein gene product 9.5; TARC, thymus and activation-regulated chemokine; TNF, tumor necrosis factor; TIMP, tissue inhibitor of metalloproteinases; VEGF, vascular endothelial growth factor; TRPV1, transient receptor potential cation channel subfamily V member 1; PFA, paraformaldehyde; FSUs, Functional Spine Units; EP, endplate; ROI, region of interest; HSD, honest significance test; DRG, dorsal root ganglion; CX3CL1, C-X3-C motif 1; VEGFA, vascular endothelial growth factor A; DAPI, 4′,6-diamidino-2-phenylindole; EDTA, ethylenediaminetetraacetic acid; ANOVA, analysis of variance; EPO, Erythropoietin.

Availability of Data and Materials

The data that support the findings of this study are available from the corresponding author upon request.

Author Contributions

REW, CEG, and SYT contributed to the design of this work and drafted the work. REW, KSB, LJ, CEG, RSP, and SYT contributed to the interpretation of data. REW, KSB, LJ, RSP, CEG, ATB, ELS, MCG, LAS, and SYT analyzed the data. REW, KSB, RSP, LJ, ATB, ELS, MCG, LAS, and SYT reviewed the manuscript critically for important intellectual content. All authors read and approved the final manuscript. All authors agreed to be accountable for all aspects of the work in ensuring that questions related

to the accuracy or integrity of any part of the work were appropriately investigated and resolved.

Ethics Approval and Consent to Participate

All animal procedures were performed with Washington University School of Medicine IACUC approval (Animal Protocol ID: 22-0292).

Acknowledgments

We gratefully acknowledge the support of the histology, structure and strength, and animal behavior Research Service Cores of Washington University Musculoskeletal Research Center (P30AR074992). Multiplex Luminex cytokine panels were analyzed by Eve Technologies Corp.

Funding

This work was conducted with funding support from National Institute of Health: R01AR074441, R01AR077678, R21AR081517, T32DK108742, and P30AR074992.

Conflict of Interest

The authors declare no conflict of interest. This article has been uploaded as a pre-print (https://www.biorxiv.org/content/10.1101/2024.07.12.603182v2).

Supplementary Material

Supplementary material associated with this article can be found, in the online version, at https://doi.org/10.22203/eCM.v054a05.

References

[1] Hoy D, March L, Brooks P, Blyth F, Woolf A, Bain C, *et al*. The global burden of low back pain: estimates from the Global Burden of Disease 2010 study. Annals of the Rheumatic Diseases. 2014; 73: 968–974. https://doi.org/10.1136/annrheumdis-2013-204428.

[2] Luoma K, Riihimäki H, Luukkonen R, Raininko R, Viikari-Juntura E, Lamminen A. Low back pain in relation to lumbar disc degeneration. Spine. 2000; 25: 487–492. https://doi.org/10.1097/00007632-200002150-00016.

[3] DePalma MJ, Ketchum JM, Saullo T. What is the source of chronic low back pain and does age play a role? Pain Medicine: the Official Journal of the American Academy of Pain Medicine. 2011; 12: 224–233. https://doi.org/10.1111/j.1526-4637.2010.01045.x.

[4] Peng BG. Pathophysiology, diagnosis, and treatment of discogenic low back pain. World Journal of Orthopedics. 2013; 4: 42–52. https://doi.org/10.5312/wjo.v4.i2.42.

[5] Zehra U, Tryfonidou M, Iatridis JC, Illien-Jünger S, Mwale F, Samartzis D. Mechanisms and clinical implications of intervertebral disc calcification. Nature Reviews. Rheumatology. 2022; 18: 352–362. https://doi.org/10.1038/s41584-022-00783-7.

[6] Fine N, Lively S, Séguin CA, Perruccio AV, Kapoor M, Rampersaud R. Intervertebral disc degeneration and osteoarthritis: a common molecular disease spectrum. Nature Reviews. Rheumatology. 2023; 19: 136–152. https://doi.org/10.1038/s41584-022-00888-z.

[7] Phillips KL, Chiverton N, Michael AL, Cole AA, Breakwell LM, Haddock G, *et al*. The cytokine and chemokine expression profile of nucleus pulposus cells: Implications for degeneration and regeneration of the intervertebral disc. Arthritis Research & Therapy. 2013; 15: R213. https://doi.org/10.1186/ar4408.

[8] Risbud MV, Shapiro IM. Role of cytokines in intervertebral disc degeneration: pain and disc content. Nature Reviews. Rheumatology. 2014; 10: 44–56. https://doi.org/10.1038/nrrheum.2013.160.

[9] Lama P, Le Maitre CL, Harding IJ, Dolan P, Adams MA. Nerves and blood vessels in degenerated intervertebral discs are confined to physically disrupted tissue. Journal of Anatomy. 2018; 233: 86–97. https://doi.org/10.1111/joa.12817.

[10] Binch AL, Cole AA, Breakwell LM, Michael AL, Chiverton N, Creemers LB, *et al.* Nerves are more abundant than blood vessels in the degenerate human intervertebral disc. Arthritis Research & Therapy. 2015; 17: 370. https://doi.org/10.1186/s13075-015-0889-6.

[11] Silva MJ, Holguin N. Aging aggravates intervertebral disc degeneration by regulating transcription factors toward chondrogenesis. FASEB Journal: Official Publication of the Federation of American Societies for Experimental Biology. 2020; 34: 1970–1982. https://doi.org/10.1096/fj.201902109R.

[12] Le Maitre CL, Hoyland JA, Freemont AJ. Catabolic cytokine expression in degenerate and herniated human intervertebral discs: IL-1beta and TNFalpha expression profile. Arthritis Research & Therapy. 2007; 9: R77. https://doi.org/10.1186/ar2275.

[13] Kikuchi T, Nakamura T, Ikeda T, Ogata H, Takagi K. Monocyte chemoattractant protein-1 in the intervertebral disc. A histologic experimental model. Spine. 1998; 23: 1091–1099. https://doi.org/10.1097/00007632-199805150-00003.

[14] Haro H, Shinomiya K, Komori H, Okawa A, Saito I, Miyasaka N, *et al*. Upregulated expression of chemokines in herniated nucleus pulposus resorption. Spine. 1996; 21: 1647–1652. https://doi.org/10.1097/00007632-199607150-00006.

[15] Bohaud C, Johansen MD, Jorgensen C, Kremer L, Ipseiz N, Djouad F. The Role of Macrophages During Mammalian Tissue Remodeling and Regeneration Under Infectious and Non-Infectious Conditions. Frontiers in Immunology. 2021; 12: 707856. https://doi.org/10.3389/fimmu.2021.707856.

[16] Burke JG, Watson RW, McCormack D, Dowling FE, Walsh MG, Fitzpatrick JM. Intervertebral discs which cause low back pain secrete high levels of proinflammatory mediators. The Journal of Bone and Joint Surgery. British Volume. 2002; 84: 196–201. https://doi.org/10.1302/0301-620x.84b2.12511.

[17] White FA, Wilson NM. Chemokines as pain mediators and modulators. Current Opinion in Anaesthesiology. 2008; 21: 580–585. https://doi.org/10.1097/ACO.0b013e32830eb69d.

[18] Easson GWD, Savadipour A, Gonzalez C, Guilak F, Tang SY. TRPV4 differentially controls inflammatory cytokine networks during static and dynamic compression of the intervertebral disc. JOR Spine. 2023; 6: e1282. https://doi.org/10.1002/jsp2.1282.

[19] Easson GWD, Savadipour A, Anandarajah A, Iannucci LE, Lake SP, Guilak F, *et al*. Modulation of TRPV4 protects against degeneration induced by sustained loading and promotes matrix synthesis in the intervertebral disc. FASEB Journal: Official Publication of the Federation of American Societies for Experimental Biology. 2023; 37: e22714. https://doi.org/10.1096/fj.202201388R.

[20] Paul CPL, Schoorl T, Zuiderbaan HA, Zandieh Doulabi B, van der Veen AJ, van de Ven PM, *et al.* Dynamic and static overloading induce early degenerative processes in caprine lumbar intervertebral discs. PloS One. 2013; 8: e62411. https://doi.org/10.1371/journal.pone.0062411.

[21] MacLean JJ, Lee CR, Grad S, Ito K, Alini M, Iatridis JC. Effects of immobilization and dynamic compression on intervertebral disc cell gene expression *in vivo*. Spine. 2003; 28: 973–981. https://doi.org/10.1097/01.BRS.0000061985.15849.A9.

[22] Lee S, Millecamps M, Foster DZ, Stone LS. Long-term histological analysis of innervation and macrophage infiltration in a mouse model of intervertebral disc injury-induced low back pain. Journal of Orthopaedic Research: Official Publication of the Orthopaedic

Research Society. 2020; 38: 1238–1247. https://doi.org/10.1002/jor.24560.

[23] Millecamps M, Lee S, Foster DZ, Stone LS. Disc degeneration spreads: long-term behavioural, histologic and radiologic consequences of a single-level disc injury in active and sedentary mice. European Spine Journal: Official Publication of the European Spine Society, the European Spinal Deformity Society, and the European Section of the Cervical Spine Research Society. 2021; 30: 2238–2246. https://doi.org/10.1007/s00586-021-06893-2.

[24] Millecamps M, Stone LS. Delayed onset of persistent discogenic axial and radiating pain after a single-level lumbar intervertebral disc injury in mice. Pain. 2018; 159: 1843–1855. https://doi.org/10.1097/j.pain.0000000000001284.

[25] Orita S, Ohtori S, Taniguchi A, Yamashita M, Yamauchi K, Inoue G, *et al*. Direct evidence for sensory innervation of the dorsal portion of the Co5/6 coccygeal intervertebral disc in rats. Spine. 2010; 35: 1346–1352. https://doi.org/10.1097/BRS.0b013e3181c099b0.

[26] Mohd Isa IL, Abbah SA, Kilcoyne M, Sakai D, Dockery P, Finn DP, *et al*. Implantation of hyaluronic acid hydrogel prevents the pain phenotype in a rat model of intervertebral disc injury. Science Advances. 2018; 4: eaaq0597. https://doi.org/10.1126/sciadv.aaq0597.

[27] Martin JT, Gorth DJ, Beattie EE, Harfe BD, Smith LJ, Elliott DM. Needle puncture injury causes acute and long-term mechanical deficiency in a mouse model of intervertebral disc degeneration. Journal of Orthopaedic Research: Official Publication of the Orthopaedic Research Society. 2013; 31: 1276–1282. https://doi.org/10.1002/jor.22355.

[28] Han B, Zhu K, Li FC, Xiao YX, Feng J, Shi ZL, *et al*. A simple disc degeneration model induced by percutaneous needle puncture in the rat tail. Spine. 2008; 33: 1925–1934. https://doi.org/10.1097/BRS.0b013e31817c64a9.

[29] Xia D, Yan M, Yin X, Hu W, Zhang C, Hu B, *et al*. A Novel Rat Tail Needle Minimally Invasive Puncture Model Using Three-Dimensional Printing for Disk Degeneration and Progressive Osteogenesis Research. Frontiers in Cell and Developmental Biology. 2021; 9: 587399. https://doi.org/10.3389/fcell.2021.587399.

[30] Leimer EM, Gayoso MG, Jing L, Tang SY, Gupta MC, Setton LA. Behavioral Compensations and Neuronal Remodeling in a Rodent Model of Chronic Intervertebral Disc Degeneration. Scientific Reports. 2019; 9: 3759. https://doi.org/10.1038/s41598-019-39657-6.

[31] Lai A, Moon A, Purmessur D, Skovrlj B, Laudier DM, Winkelstein BA, *et al*. Annular puncture with tumor necrosis factor-alpha injection enhances painful behavior with disc degeneration *in vivo*. The Spine Journal: Official Journal of the North American Spine Society. 2016; 16: 420–431. https://doi.org/10.1016/j.spinee.2015.11.019.

[32] Michalek AJ, Funabashi KL, Iatridis JC. Needle puncture injury of the rat intervertebral disc affects torsional and compressive biomechanics differently. European Spine Journal: Official Publication of the European Spine Society, the European Spinal Deformity Society, and the European Section of the Cervical Spine Research Society. 2010; 19: 2110–2116. https://doi.org/10.1007/s00586-010-1473-z.

[33] Walk RE, Moon HJ, Tang SY, Gupta MC. Contrast-enhanced microCT evaluation of degeneration following partial and full width injuries to the mouse lumbar intervertebral disc. Scientific Reports. 2022; 12: 15555. https://doi.org/10.1038/s41598-022-19487-9.

[34] Qiu S, Shi C, Anbazhagan AN, Das V, Arora V, Kc R, *et al*. Absence of VEGFR-1/Flt-1 signaling pathway in mice results in insensitivity to discogenic low back pain in an established disc injury mouse model. Journal of Cellular Physiology. 2020; 235: 5305–5317. https://doi.org/10.1002/jcp.29416.

[35] Shi C, Das V, Li X, Kc R, Qiu S, O-Sullivan I, *et al*. Development of an *in vivo* mouse model of discogenic low back pain. Journal of Cellular Physiology. 2018; 233: 6589–6602. https://doi.org/10.1002/jcp.26280.

[36] Tian Z, Ma X, Yasen M, Mauck RL, Qin L, Shofer FS, *et al*. Intervertebral Disc Degeneration in a Percutaneous Mouse Tail Injury Model. American Journal of Physical Medicine & Rehabilitation/Association of Academic Physiatrists. 2018; 97: 170–177. https://doi.org/10.1097/PHM.0000000000000818.

[37] The Anatomy of the Laboratory Mouse. 2024. Available at: https://www.informatics.jax.org/cookbook/ (Accessed: 22 May 2024).

[38] Vincent K, Mohanty S, Pinelli R, Bonavita R, Pricop P, Albert TJ, *et al*. Aging of mouse intervertebral disc and association with back pain. Bone. 2019; 123: 246–259. https://doi.org/10.1016/j.bone.2019.03.037.

[39] Melgoza IP, Chenna SS, Tessier S, Zhang Y, Tang SY, Ohnishi T, *et al*. Development of a standardized histopathology scoring system using machine learning algorithms for intervertebral disc degeneration in the mouse model-An ORS spine section initiative. JOR Spine. 2021; 4: e1164. https://doi.org/10.1002/jsp2.1164.

[40] Blondel VD, Guillaume JL, Lambiotte R, Lefebvre E. Fast unfolding of communities in large networks. Journal of Statistical Mechanics Theory and Experiment. 2008; 10: 10008–10020. https://doi.org/10.1088/1742-5468/2008/10/P10008.

[41] Arshadi C, Günther U, Eddison M, Harrington KIS, Ferreira TA. SNT: a unifying toolbox for quantification of neuronal anatomy. Nature Methods. 2021; 18: 374–377. https://doi.org/10.1038/s41592-021-01105-7.

[42] Gansau J, Grossi E, Rodriguez L, Wang M, Laudier DM, Chaudhary S, *et al*. TNFR1-mediated senescence and lack of TNFR2-signaling limit human intervertebral disc cell repair potential in degenerative conditions. Osteoarthritis and Cartilage/OARS, Osteoarthritis Research Society. 2025; 33: 874–887. https://doi.org/10.1016/j.joca.2025.02.791.

[43] Wang Y, Che M, Xin J, Zheng Z, Li J, Zhang S. The role of IL-1β and TNF-α in intervertebral disc degeneration. Biomedicine & Pharmacotherapy = Biomédecine & Pharmacothérapie. 2020; 131: 110660. https://doi.org/10.1016/j.biopha.2020.110660.

[44] Olmarker K, Iwabuchi M, Larsson K, Rydevik B. Walking analysis of rats subjected to experimental disc herniation. European Spine Journal: Official Publication of the European Spine Society, the European Spinal Deformity Society, and the European Section of the Cervical Spine Research Society. 1998; 7: 394–399. https://doi.org/10.1007/s005860050096.

[45] Huang Y, Lei L, Zhu J, Zheng J, Li Z, Wang H, *et al*. Pain behavior and phenotype in a modified anterior lumbar disc puncture mouse model. JOR Spine. 2023; 7: e1284. https://doi.org/10.1002/jsp2.1284.

[46] Barbe MF, Chen FL, Loomis RH, Harris MY, Kim BM, Xie K, *et al*. Characterization of pain-related behaviors in a rat model of acute-to-chronic low back pain: single vs. multi-level disc injury. Frontiers in Pain Research. 2024; 5: 1394017. https://doi.org/10.3389/fpain.2024.1394017.

[47] Tannenbaum J, Bennett BT. Russell and Burch's 3Rs then and now: the need for clarity in definition and purpose. Journal of the American Association for Laboratory Animal Science: JAALAS. 2015; 54: 120–132.

[48] Yang F, Leung VYL, Luk KDK, Chan D, Cheung KMC. Injury-induced sequential transformation of notochordal nucleus pulposus to chondrogenic and fibrocartilaginous phenotype in the mouse. The Journal of Pathology. 2009; 218: 113–121. https://doi.org/10.1002/path.2519.

[49] Piazza M, Peck SH, Gullbrand SE, Bendigo JR, Arginteanu T, Zhang Y, *et al*. Quantitative MRI correlates with histological grade in a percutaneous needle injury mouse model of disc degeneration. Journal of Orthopaedic Research: Official Publication of the Orthopaedic Research Society. 2018; 36: 2771–2779. https://doi.org/10.1002/jor.24028.

[50] Kang JD, Georgescu HI, McIntyre-Larkin L, Stefanovic-Racic M, Evans CH. Herniated cervical intervertebral discs spontaneously produce matrix metalloproteinases, nitric oxide, interleukin-6, and prostaglandin E2. Spine. 1995; 20: 2373–2378. https://doi.org/10.

1097/00007632-199511001-00001.
[51] Gawri R, Rosenzweig DH, Krock E, Ouellet JA, Stone LS, Quinn TM, *et al*. High mechanical strain of primary intervertebral disc cells promotes secretion of inflammatory factors associated with disc degeneration and pain. Arthritis Research & Therapy. 2014; 16: R21. https://doi.org/10.1186/ar4449.
[52] Sokol CL, Luster AD. The chemokine system in innate immunity. Cold Spring Harbor Perspectives in Biology. 2015; 7: a016303. https://doi.org/10.1101/cshperspect.a016303.
[53] Dimberg A. Chemokines in angiogenesis. Current Topics in Microbiology and Immunology. 2010; 341: 59–80. https://doi.org/10.1007/82_2010_21.
[54] Li Z, Liu H, Yang H, Wang J, Wang H, Zhang K, *et al*. Both expression of cytokines and posterior annulus fibrosus rupture are essential for pain behavior changes induced by degenerative intervertebral disc: An experimental study in rats. Journal of Orthopaedic Research: Official Publication of the Orthopaedic Research Society. 2014; 32: 262–272. https://doi.org/10.1002/jor.22494.
[55] Zhang J, Li Z, Chen F, Liu H, Wang H, Li X, *et al*. TGF-β1 suppresses CCL3/4 expression through the ERK signaling pathway and inhibits intervertebral disc degeneration and inflammation-related pain in a rat model. Experimental & Molecular Medicine. 2017; 49: e379. https://doi.org/10.1038/emm.2017.136.
[56] Mesquida-Veny F, Hervera A. Neuronal chemokines: new insights into neuronal communication after injury. Neural Regeneration Research. 2023; 18: 2379–2380. https://doi.org/10.4103/1673-5374.371352.
[57] Urbantat RM, Blank A, Kremenetskaia I, Vajkoczy P, Acker G, Brandenburg S. The CXCL2/IL8/CXCR2 Pathway Is Relevant for Brain Tumor Malignancy and Endothelial Cell Function. International Journal of Molecular Sciences. 2021; 22: 2634. https://doi.org/10.3390/ijms22052634.
[58] Mehrad B, Keane MP, Strieter RM. Chemokines as mediators of angiogenesis. Thrombosis and Haemostasis. 2007; 97: 755–762.
[59] Silva JR, Iftinca M, Gomes FIF, Segal JP, Smith OMA, Bannerman CA, *et al*. Skin-resident dendritic cells mediate postoperative pain via CCR4 on sensory neurons. Proceedings of the National Academy of Sciences of the United States of America. 2022; 119: e2118238119. https://doi.org/10.1073/pnas.2118238119.
[60] Allen KD, Griffin TM, Rodriguiz RM, Wetsel WC, Kraus VB, Huebner JL, *et al*. Decreased physical function and increased pain sensitivity in mice deficient for type IX collagen. Arthritis and Rheumatism. 2009; 60: 2684–2693. https://doi.org/10.1002/art.24783.
[61] Krames ES. The role of the dorsal root ganglion in the development of neuropathic pain. Pain Medicine: the Official Journal of the American Academy of Pain Medicine. 2014; 15: 1669–1685. https://doi.org/10.1111/pme.12413.
[62] Clayton SW, Walk RE, Mpofu L, Easson GWD, Tang SY. Sex-specific divergences in the types and timing of infiltrating immune cells during the intervertebral disc acute injury response and their associations with degeneration. Osteoarthritis and Cartilage/OARS, Osteoarthritis Research Society. 2025; 33: 247–260. https://doi.org/10.1016/j.joca.2024.10.002.
[63] Rohanifar M, Clayton SW, Easson GWD, Patil DS, Lee F, Jing L, *et al*. Single Cell RNA-Sequence Analyses Reveal Uniquely Expressed Genes and Heterogeneous Immune Cell Involvement in the Rat Model of Intervertebral Disc Degeneration. Applied Sciences. 2022; 12: 8244. https://doi.org/10.3390/app12168244.
[64] Burt KG, Kim MKM, Viola DC, Abraham AC, Chahine NO. Nuclear factor κB overactivation in the intervertebral disc leads to macrophage recruitment and severe disc degeneration. Science Advances. 2024; 10: eadj3194. https://doi.org/10.1126/sciadv.adj3194.

Editor's note: The Scientific Editor responsible for this paper was Sibylle Grad.

Received: 1st November 2024; **Accepted**: 23rd September 2025; **Published**: 31st December 2025